Chinese Journal of Chemical Engineering 65 (2024) 106–116

Contents lists available at ScienceDirect

Chinese Journal of Chemical Engineering

journal homepage: www.elsevier.com/locate/CJChE

Full Length Article

Investigation of oxy-fuel combustion for methane and acid gas in a diffusion flame

Songling Guo, Xun Tao, Fan Zhou, Mengyan Yu, Yufan Wu, Yunfei Gao, Lu Ding, Fuchen Wang *

Institute of Clean Coal Technology, East China University of Science and Technology, Shanghai 200237, China

ARTICLE INFO

Article history:
Received 7 December 2022
Received in revised form 4 July 2023
Accepted 4 July 2023
Available online 29 August 2023

Keywords:
Acid gas
Methane
Oxy-fuel combustion
Oxidation
Chemical analysis
Carbon sulfides

ABSTRACT

Co-combustion of methane (CH_4) and acid gas (AG) is required to sustain the temperature in Claus reaction furnace. In this study, oxy-fuel combustion of methane and acid gas has been experimentally studied in a diffusion flame. Three equivalence ratios (ER = 1.0, 1.5, 2.0) and CH_4-addition ratios (CH_4/AG = 0.3, 0.5, 0.7) were examined and the flame was interpreted by analyzing the distributions of the temperature and species concentration along central axial. CH_4-AG diffusion flame could be classified into three sections namely initial reaction, oxidation and complex reaction sections. Competitive oxidation of CH_4 and H_2S was noted in the first section wherein H_2S was preferred and both were mainly proceeding decomposition and partial oxidation. SO_2 was formed at oxidation section together with obvious presence of H_2 and CO. However, H_2 and CO were inclined to be sustained under fuel rich condition in the complex reaction section. Reducing ER and increasing CH_4/AG contributed to higher temperature, H_2S and CH_4 oxidation and CO_2 reactivity. Hence a growing trend for CH_4 and AG to convert into H_2, CO and SO_2 could be witnessed. And this factor enhanced the generation of CS_2 and COS in the flame inner core by interactions of CH_4 and CO_2 with sulfur species. COS was formed through the interactions of CO and CO_2 with sulfur species. The CS_2 production directly relied on reaction of CH_4 with sulfur species. The concentration of COS was greater than CS_2 since CS_2 was probably inhibited due to the presence of H_2. COS and CS_2 could be consumed by further oxidation or other complex reactions.

1. Introduction

Hydrogen sulfide, a flammable and toxic gas, is widely spotted in crude natural gas, petroleum well and coal seams and is a common by-product during a number of industries such as coal or biomass gasification, oil refining, gas sweetening, biogas utilization, waste gas purification, waste water treatment and other desulfurization processes [1–4]. Generally, acid gas (AG) mainly consists of H_2S and CO_2 and other impurities with low concentration such as hydrocarbons, NH_3 and CS_2 and COS [3,4]. Meanwhile, it is well known that venting acid gas or its combustion products (mainly SO_2) directly into atmosphere without any post processing is forbidden since it can cause various environmental pollution and health hazards [5]. Therefore, acid gas must be processed properly to meet the increasingly strict regulations and consideration of environment and safety. Currently, the modified Claus process is widely used for the treatment of acid gas and the recovery of economically valuable sulfur products [1,6]. This process consists of three consecutive sections. In the first step, the oxidation of H_2S to SO_2 (Eq. (1)) and the Claus reaction between H_2S and SO_2 (Eq. (2)) to form sulfur (mainly S_2) occur simultaneously at over 1273 K in the reaction furnace [7]. The second part is a further Claus reaction (Eq. (3)) occurring over catalyst bed at about 573 K in the catalytic converters, rendering S_8 as the primary product [8,9]. The final section is the tail gas treatment or incinerating to meet emission standards. The reactions of the Claus process can be described as follows:

$$H_2S + 1.5O_2 \rightarrow SO_2 + H_2O \quad \Delta H_r = -520.72\,kJ \cdot mol^{-1} \tag{1}$$

$$2H_2S + SO_2 \rightarrow 1.5S_2 + 2H_2O \quad \Delta H_r = 42.45\,kJ \cdot mol^{-1} \tag{2}$$

$$2H_2S + SO_2 \rightarrow 3/8S_8 + 2H_2O \quad \Delta H_r = -104\,kJ \cdot mol^{-1} \tag{3}$$

The partial oxidation of H_2S in the reaction furnace is deemed as the most critical and complex section for the Claus process [10–13]. It includes the generation of up to approximately 70% sulfur and adjustment of the suitable H_2S/SO_2 ratio for subsequent catalytic reaction [14,15]. Meanwhile, the impurities in acid gas

* Corresponding author.
E-mail address: wfch@ecust.edu.cn (F. Wang).

https://doi.org/10.1016/j.cjche.2023.07.009
1004-9541/

need to be destroyed to mitigate the negative impact on the catalytic section. However, this process is hard to achieve since the CH_4 co-combustion is required to maintain the furnace temperature especially when the H_2S content is below 50% [16,17]. The presence of additional CH_4 and pre-existing CO_2 can significantly complicate the reactions in the reaction furnace and further adversely affect the Claus reaction. Not only is there competitive oxidation of H_2S and CH_4, but unwanted COS and CS_2 from various side reactions and soot also proceed in the combustion progress, which can degrade catalyst performance and reduce the sulfur recovery efficiency once existing in the catalytic section due to the sulfate corrosion and coverage on the catalytic pores [18,19].

To understand the effects of CH_4 and CO_2 on partial oxidation of H_2S in the reaction furnace, researchers have been conducting intensively studies in recent decades [20–24]. Li *et al.* [18] has studied the oxidation process of acid gas in a non-premixed flame. As the reactivity in fuel-rich condition was mainly expressed as $CO_2 + H \rightleftharpoons CO + OH$, especially at high temperature, CO_2 could reduce the H/OH ratio by converting atomic H into OH radical. Meanwhile enhancing oxygen concentration (OC) would raise the flame temperature, accelerate the oxidation of H_2S and promote the generation of CO at near-burner region. Selim *et al.* [25] has investigated the effect of CO_2 on H_2S combustion in a diffusion flame and found that the addition of CO_2 resulted a drop in flame temperature but contributed to raise downstream temperature. They also summarized the impact of CO_2 for flame temperature was attributed to its oxidizing medium role in the reaction pool. This was consistent with the results that studied by Ibrahim and Raj [26]. Moreover, Lee *et al.* [27] concluded the primary chemical effects of CO_2 on flame were its collisional decomposition and pyrolysis, and highlighted the significance of CO_2 in preventing heat dissipation. In general, the CO_2 reactivity cannot be ignored during AG combustion. Moreover, compared with CO_2, the impact of CH_4 on H_2S oxidation could be more profound and complicated. Based on the study of H_2S flame structure by Bernez-Cambot *et al.* [28], Li *et al.* [15] investigated the oxidation of H_2S and CH_4 mixture at 1:1 in different ERs (1.0, 1.4, 2.0) and divided the diffusion flame into three zones: the initial oxidation, the intense burning and the afterburning zones. In the initial oxidation zone, H_2S was dominant in the competitive oxidation with CH_4 injecting at the base of the flame, and it was inferred that H_2S was mainly partially oxidized in this process. The mixing and combustion were contained in the second zone wherein major reaction heat was released and CO_2, SO_2 and H_2O were substantially formed. The third zone incorporated complex reactions and the Claus reaction (Eq. (2)). Meanwhile Karan *et al.* [29] discussed CH_4 was only partially consumed in the flame zone and its main conversion process occurred in the anaerobic zone at the post-flame. Colom-Díaz *et al.* [30] further highlighted the competitive advantage of H_2S over CH_4 to be more significant at high pressures. Similar to CH_4, Ibrahim *et al.* [31–33] has investigated the effect of high hydrocarbon substances represented by BTEX (benzene, toluene, ethylbenzene and xylene) on H_2S combustion under Claus condition and found that BTEX significantly promoted the formation of H_2. However, H_2 hindered the oxidation of H_2S and the production of SO_2, which in turn affected the sulfur yield. The production of COS and CS_2 was also improved since the favorable production of CO and could react rapidly with S_2 or SO_2 to produce COS. It was consistent with the conclusion of Palma *et al.* [34]. Selim *et al.* [35] conducted an experimental study of the oxidation of H_2S in a CH_4–air flame and found trace amounts of high hydrocarbons were generated under Claus condition (ER = 3) wherein SO_2 performed as a coupling catalyst, enhancing the combination of CH_3 and forming hydrocarbons. This group also considered the formation of CS_2 from CH_4 and sulfur-containing substances is more favorable in anoxic environment.

Much of the previous interest of CH_4/CO_2 chemistry has evidently stated the relationship between CH_4/CO_2 and COS/CS_2. Chin *et al.* [36] studied the oxidation of H_2S–CH_4 gas mixture in a tubular reactor at 1273–1473 K. They found the presence of CH_4 led to faster consumption of H_2S and production of CS_2. Abián *et al.* [19] conducted research about the conversion of COS and CS_2 and emphasized the role of CS radical in the production CS_2, primarily *via* reacting with sulfur species such as S, S_2 or SH. The large amount of CH decomposed by hydrocarbon substances plays a significant role in promoting the formation of CS_2 *via* $CH + 2H_2S \rightleftharpoons CS_2 + 2.5H_2$. Regarding the COS formation, Clark *et al.* [37] emphasized that CO, despite the presence of CO_2, was the direct source to generate COS chiefly through $CO + 0.5S_2 \rightleftharpoons COS$ and $CO + H_2S \rightleftharpoons COS + H_2$ in the Claus furnace. This viewpoint was in line with the homogeneous gas phase research in H_2S–CO_2 and H_2S–CO systems from Karan *et al.* [38]. Besides, Li *et al.* [20,21] discussed the pathway of $CH_3 \rightarrow CH_2S \rightarrow HCS \rightarrow CS \rightarrow CS_2$ in the experimental and mechanistic study of the H_2S–CH_4 system, whereas in the H_2S–CO_2 system the conversion of CS_2 from COS was emphasized. Meanwhile, the presence of reducing and oxidizing substances is an obvious factor in the tight conversion between COS and CS_2 [39,40]. It can be assumed that the generation of COS and CS_2 in the H_2S–CO_2–CH_4 system could be more complex than that of simply H_2S-CO_2 or H_2S-CH_4. However, little attention has been paid to this integrated system, which more closely resembles the real environment of the reaction furnace. Moreover, the effect of CH_4 on the oxidation of acid gas (H_2S and CO_2) under oxy-fuel combustion was less investigated and the generation of COS and CS_2 in H_2S-rich diffusion flame was still not understood since the previous literatures mostly investigated the H_2S reaction through detailed mechanisms or adding rare amount of H_2S to other combustibles [13,19,24,29,37]. To fill this gap, we aim to study the body knowledge involving CH_4–AG rich diffusion flame and oxy-fuel combustion.

The experiment was conducted using a coaxial burner in a vertical reactor wherein three equivalence ratios (ER = 1.0, 1.5, 2.0) and CH_4 addition ratios (CH_4/AG = 0.3, 0.5, 0.7) were examined to explore the oxy-fuel combustion behavior of CH_4 and AG. The reasons for choosing pure oxygen as oxidant also include its ability to make the combustion easier to observe and to overcome the concentration errors caused by interference from N_2 in the air or oxygen-enriched air. The temperature and concentration distribution of species (H_2S, CH_4, CO, CO_2, SO_2, H_2, COS, CS_2) in central axis were measured and a detailed description regarding the conversion and formation of species was presented under varies feeding modes.

2. Materials and Methods

2.1. Experimental setup

Fig. 1 shows the schematic diagram of the experimental setup. The system consists of gas cylinders, mass flow controllers, quartz tube reactor, motor programming controller, temperature monitor, gas component analysis and tail gas treatment. The reactor has an inner diameter of 90 mm, a length of 300 mm and a thickness of 5 mm, with a 15 mm thick layer of fine quartz cotton wrapped around the outside for insulation. A double concentric tubular burner, with an annular obtuse body at the upper end of the central passage, is installed in the center of the bottom of the reactor to ensure a stable flame. H_2S (99.9%, purity), CO_2 (99.9%) and CH_4 (99.5%) are regulated *via* mass flow controllers, mixed thoroughly

in a longer pipe and fed into the central passage of the burner. The oxidant of O_2 (99.9%) is fed into the annular gap passage of the burner. N_2 (99.9%) is the safe gas after the experiment procedure. Noted that the cabinet for gas cylinders of H_2S, CH_4 and CO_2 are placed at opposite corner of the laboratory to gas cylinders of O_2 and N_2.

Partial combustion of $H_2S/CO_2/CH_4$ produces sulfur/soot that could condense and adhere to the quartz wall, thus it is extremely difficult to illustrate the shape of the flame using a high-speed camera. Being a toxic gas, it is dangerous to combust directly without the reactor to take clear pictures of the flame. Therefore, thermocouple and quartz tube were used to obtain the central axial temperature and concentration distribution of the gas components in the reactor [18,31]. A motor programming controller was used to control the up and down movement of the module on the rail. By fixing a thermocouple/quartz tube on the module, temperature measurement or sampling was achieved. Noted that the temperature measurement and gas sampling were not carried out simultaneously, but twice for the same experimental condition. The thermocouple was a K-type thermocouple with a 2.3 mm diameter bead. The detected points for gas samples were chosen to be 10, 25, 40, 55, 70, 85, 100, 115 and 130 mm from the burner exit and for temperature measurement were considered more in the flame zone to outline a clear distribution. The combustion was considered to be stable when the temperature fluctuated by less than 3 K within 30 s and the temperature measurement data was recorded by a temperature monitor. Gas samples were taken at a rate of 2 $ml \cdot s^{-1}$ from each detected point using a thin quartz tube (2.2 mm inner diameter, 4 mm outer diameter), and accessed to air bags after three consecutive gas treatments in gas washing bottles, *i.e.* quenching through water, sulfur separation *via* fine quartz wool and drying in silica gel bottle. Fine syringes were used to pump gas from air bags into GC (gas chromatograph) analysis for analyzing component concentrations. The tail gas was treated with sulfur trap and NaOH solution, then discharged into a negative pressure ventilation system.

In GC analysis, a thermal conductivity detector (TCD) in series with a flame photometric detector (FPD, column type GDX-303) was used to determine the concentration of sulfur-containing substances, where the column was maintained at 339 K. The concentration of non-sulfur components was determined in tandem with a chromatographic column. Between TCD and FID was a converter equipped with an active nickel catalyst, which contributed to accurately measure the concentration of CO and CO_2 at a column temperature of 333 K and a catalytic oven temperature of 593 K.

The experiment was conducted in a fume hood after checking the fixed alarms and pipeline gas tightness. Experimenters must wear gas masks and body alarms, and the laboratory need to be kept ventilated. Considering the toxicity of H_2S, acid gas cannot be directly ignited at the beginning of the experiment. To deal with this difficulty, CH_4 was firstly injected and flamed. After the flame was stabilized, H_2S and CO_2 were slowly injected and the flame color gradually changed from yellow to blue. This phenomenon showed the H_2S started to flame. Afterwards, each gas was adjusted to the specified flow rate according to the experimental conditions. A pump with a flow meter was used to extract the gas to maintain stable pressure in the reactor, typically at a value of 0.6–0.7 times the inlet gas flow based on experimental experience. The control module was operated to adjust the K-type thermocouple (or sampling tube) to the specified position and the temperature (or gas sampling) was measured. The experiment was stopped by closing the H_2S cylinder valve. The residual H_2S in the pipeline has been burned out before closing the CH_4 cylinder valve. Then, CH_4 was eventually consumed and the flame was extinguished. Finally, N_2 was filled with the pipeline and the fume hood was ventilated for 30 min.

2.2. Parameter definition

To have good universality, the dimensionless axial distance is defined by the following equation:

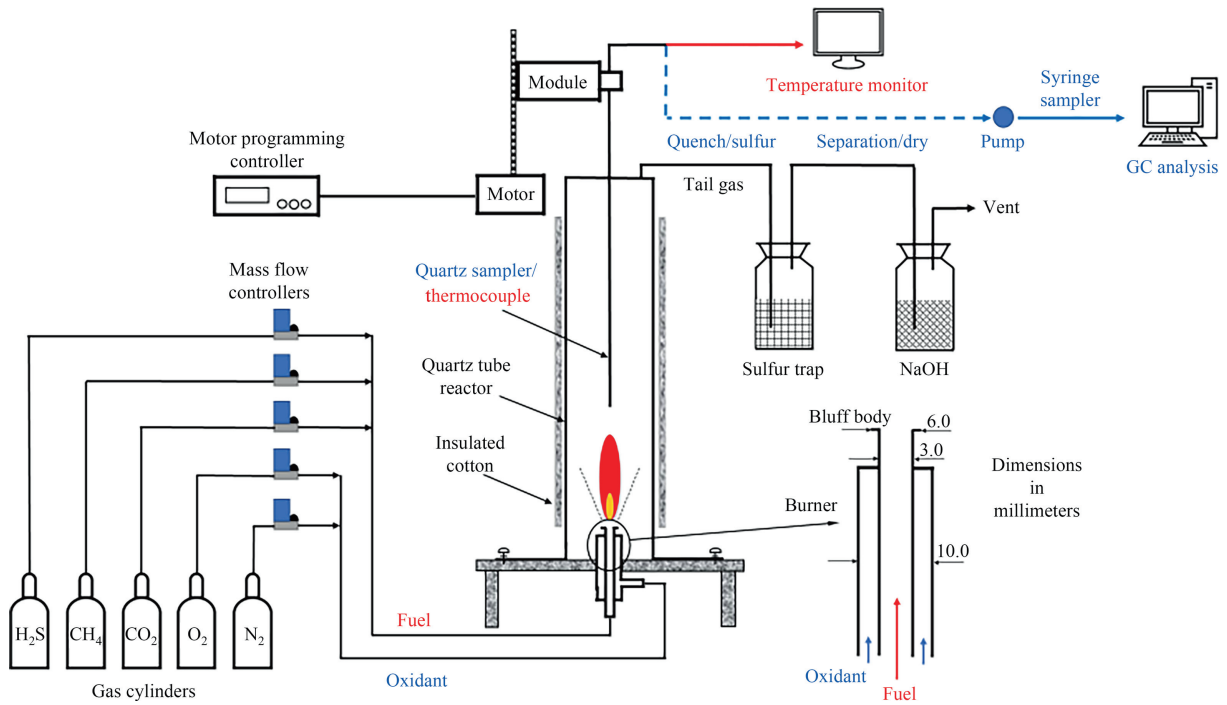

Fig. 1. Scheme diagram of experimental setup.

$$D = \frac{X}{D_0} \tag{4}$$

where D_0 is the inner diameter of the burner (D_0 = 3 mm), and X is the axial distance from the surface of the burner to the outlet (X = 0 is the surface of the burner). And equivalent ratio (ER) is given as follows:

$$\mathrm{ER} = \frac{\text{theoretical oxygen feed}}{\text{actual oxygen feed}} \tag{5}$$

The theoretical oxygen feed is the amount of O_2 that can exactly oxidize H_2S to SO_2 and CH_4 to CO_2 which is calculated as follows:

$$[\text{theoretical oxygen feed}] = 1.5[H_2S] + 2[CH_4] \tag{6}$$

2.3. Experimental conditions

Experimental conditions are presented in Table 1. Two variables of equivalence ratio (1.0, 1.5 and 2.0) and CH_4/AG (0.3, 0.5 and 0.7) were considered to study their impacts on flame temperature and the conversion and formation of main species under oxy-fuel condition.

2.4. Analysis of errors on measured temperature

2.4.1. Analysis of error on measured temperature

When the thermocouple temperature is stable, the following equation of conservation of energy should be satisfied on the surface of the beads [41]:

$$h_f(T_g - T_b) = \varepsilon\sigma\left(T_b^4 - T_w^4\right) \tag{7}$$

where T_g, T_b and T_w denote temperatures of the gas, the electric coupling bead and the reactor wall, respectively. The K-type thermocouple used in this experiment is a nickel–chromium alloy with a coupling bead emissivity of ε = 0.31 [42]. σ is the blackbody radiation constant and the value is 5.67×10^{-8} W·m^{-2}·K^{-4}. The correlation equation for the fluid outer swept sphere can be determined by the following equations [41,43]:

$$Nu = 2 + \left(0.4Re^{0.5} + 0.06Re^{2/3}\right)Pr^{0.4}\left(\frac{\mu_w}{\mu_b}\right) = \frac{D_b h_f}{\lambda} \tag{8}$$

$$Re = \frac{\rho v D_b}{\mu} \tag{9}$$

$$Pr = \frac{\mu C_p}{\lambda} \tag{10}$$

Nu, *Pr* and *Re* refer the Nussle, Prandtl and Reynolds number, respectively. μ_w and μ_b are the kinetic viscosities at wall and bead thermocouple temperatures. λ is the thermal conductivity and D_b stands for the diameter of the bead thermocouple with a value of 1.5 mm. h_f is the convective heat transfer coefficient between the electric coupling beads and the airflow. ρ, v and C_p represent the density, velocity and the heat capacity, respectively.

The calculation is based on the error of temperature measurement at the highest temperature. For example, the highest measured temperature that appears in mode A is 1262 K at D≈3 [18]. As the gas diffusion here was not completely developed near the burner, the velocity at the measured point can be obtained as approximately 7 m·s^{-1} considering the gas flow, nozzle size and airflow expansion [18]. The thermal properties of the gas mixture at the highest temperature are λ of 0.0833 W·m^{-1}·K, ρ of 0.3416 kg·m^{-3}, C_p of 2453 J·kg·K^{-3} and μ of 4.17×10^{-5} Pa·s. Hence *Re*, *Nu* and h_f are 133.57, 8.486 and 307.34 W·m^{-2}·K^{-1}. The gas temperature (T_g) is approximately 1388 K *via* Eq. (7). The relative error of mode A is 9.08% according to the following equation:

$$\varphi = \frac{T_g - T_b}{T_g} \tag{11}$$

Utilizing the same method, the gas temperatures (T_g) in modes B–F are worked out to be 1174 K, 995 K, 1063 K, 1155 K and 1198 K, respectively, and the corresponding relative errors are 6.73%, 4.72%, 5.93%, 6.15% and 6.26%, respectively.

2.4.2. Uncertainty analysis

The uncertainty of key parameters of ER and CH_4/AG ratio are calculated based on the method in Refs. [15,18]. The specific calculation steps are as follows:

$$\mathrm{ER} = \frac{\left(m_{\text{fuel}}/m_{O_2}\right)_{\text{act}}}{\left(m_{\text{fuel}}/m_{O_2}\right)_{\text{sto}}} = \left(\frac{9.52X_{CH_4}}{X_{H_2S}} + 7.14\right)\frac{V_{H_2S}}{V_{O_2}} = \left(\frac{7.14X_{H_2S}}{X_{CH_4}} + 9.52\right)\frac{V_{CH_4}}{V_{O_2}} \tag{12}$$

$$E_{\mathrm{ER}} = \frac{\sqrt{\left(\frac{\partial \mathrm{ER}}{\partial V_{H_2S}}\delta V_{H_2S}\right)^2 + \left(\frac{\partial \mathrm{ER}}{\partial V_{CH_4}}\delta V_{CH_4}\right)^2 + \left(\frac{\partial \mathrm{ER}}{\partial V_{O_2}}\delta V_{O_2}\right)^2}}{\mathrm{ER}_{\max}} \tag{13}$$

$$\frac{\partial \mathrm{ER}}{\partial V_{H_2S}} = \left(\frac{9.52X_{CH_4}}{X_{H_2S}} + 7.14\right)\frac{1}{V_{O_2,\max}} \tag{14}$$

$$\frac{\partial \mathrm{ER}}{\partial V_{CH_4}} = \left(\frac{7.14X_{H_2S}}{X_{CH_4}} + 9.52\right)\frac{1}{V_{O_2,\max}} \tag{15}$$

$$\frac{\partial \mathrm{ER}}{\partial V_{O_2}} = -\left(\frac{7.14X_{CH_4}}{X_{H_2S}} + 9.52\right)\frac{V_{CH_4,\max}}{V_{O_2,\max}^2} \tag{16}$$

$$\mathrm{ER}_{\max} = 2.0 \tag{17}$$

In the Eq. (12), m_{fuel} and m_{O_2} refer the mass flow rates of fuel and O_2, respectively. The subsets act and sto are the actual and stoichiometric data, respectively. X_{CH_4} and X_{H_2S} represent the volume

Table 1
Experimental conditions in this study

Effect of equivalence ratio					
Mode	ER	V_{H_2S}/ml·min^{-1}	V_{CO_2}/ml·min^{-1}	V_{CH_4}/ml·min^{-1}	V_{O_2}/ml·min^{-1}
A	1.0	300	200	200	850
B	1.5	300	200	200	570
C	2.0	300	200	200	425
Effect of CH_4/AG, ER = 1.6					
Mode	CH_4/AG	V_{H_2S}/ml·min^{-1}	V_{CO_2}/ml·min^{-1}	V_{CH_4}/ml·min^{-1}	V_{O_2}/ml·min^{-1}
D	0.3	300	200	150	470
E	0.5	300	200	250	530
F	0.7	300	200	350	720

fraction of CH_4 and H_2S, respectively. E_{ER} is the uncertainty of the key parameter ER. $V_{O_2,max}$ and $V_{CH_4,max}$ denote the maximum volume flow rate of O_2 and CH_4, respectively. δV is the flow control accuracy and it is 0.001 L·min^{-1} for H_2S and CH_4 and 0.01 L·min^{-1} for O_2. Hence the uncertainty of ER can be calculated to be 1.47%.

$$CH_4/AG = \frac{V_{CH_4}}{V_{H_2S} + V_{CO_2}} \tag{18}$$

$$E_{CH_4/AG} = \frac{\sqrt{\left(\frac{\partial CH_4/AG}{\partial V_{AG}}\delta V_{AG}\right)^2 + \left(\frac{\partial CH_4/AG}{\partial V_{CH_4}}\delta V_{CH_4}\right)}}{CH_4/AG_{max}} \tag{19}$$

$$\frac{\partial CH_4/AG}{\partial V_{AG}} = \frac{1}{V_{CH_4,max}} \tag{20}$$

$$\frac{\partial CH_4/AG}{\partial V_{CH_4}} = -\frac{V_{H_2S,max}}{V^2_{CH_4,max}} \tag{21}$$

$$CH_4/AG_{max} = 0.7 \tag{22}$$

Based on the equations above, the uncertainty for CH_4/AG ratio can be worked out to be 0.71%.

3. Results and Discussion

3.1. Experimental study of CH_4–AG combustion: Effect of equivalence ratio

Fig. 2 shows the temperature curves of modes A, B and C. Similar trends of temperature distributions for all modes could be noted as obvious typical diffusion flame characteristics. The axial temperature increased from burner exit to a peak value of 1262 K, 1095 K and 948 K at ER of 1.0, 1.5 and 2.0, respectively, and dropped almost linearly. This is attributed to the heat dissipation from heat convection with ambient gas and radiation with the reactor wall [18]. The flame temperature increased significantly with decreasing ER, since enhanced oxygen feed favored CH_4–AG combustion and released more heat. Furthermore, the peak axial temperature of mode A was reached at a relatively farther location compared with mode C. It could be interpreted as the increased oxygen flow rate raising the height of the core combustion zone. This also contributed to a shorter residence time and greater heat loss in the reactor. Consequently, the temperature gap between peak value and the reactor end was 412 K, 356 K and 259 K in modes A, B and C, separately.

Volume fraction distributions of H_2S and SO_2 for modes A, B and C are presented in Fig. 3. It should be noted that the initial point (D = 0) is determined by species content in the premixed fuel gas and the first sampling point is D = 3.3. The volume fraction of H_2S in all modes decreased promptly near the burner and subsequently experienced a relatively moderate conversion downstream. For the combustion of H_2S, investigators confirmed the H_2S conversion was primarily classified into chemical and thermal decomposition and oxidation [28,35,44]. Based on the distribution of temperature and SO_2 volume fraction, the chemical decomposition of H_2S, regarded as the very initial step of H_2S consumption, occurred at the vicinity of the burner exit from which SH and H_2 but not SO_2 was the primary product (Eqs. (23) and (24)) [45,46]. However, thermal decomposition of H_2S (Eq. (25)) was only likely to proceed with a relatively apparent rate in mode A since the temperature was reaching the recommend value of 1273 K [47,48].

$$H_2S + H \rightleftharpoons H_2 + SH \tag{23}$$

$$H_2S + S \rightleftharpoons 2SH \tag{24}$$

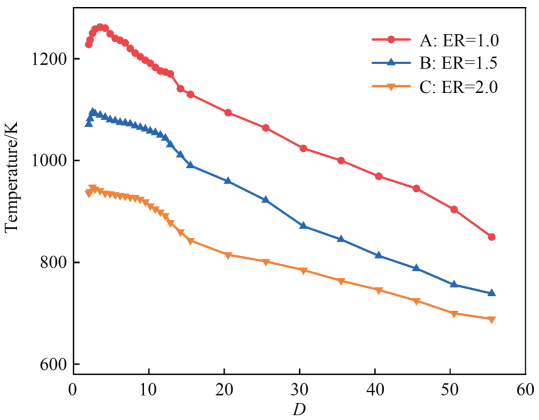

Fig. 2. Measured temperature profiles along D.

$$H_2S + M \rightleftharpoons H_2 + S + M \tag{25}$$

As the H_2S decomposition proceeded, the H_2S partial oxidation took place with the aid of radicals like O and OH (Eqs. (26) and (27)) wherein the mixing of fuel and oxidant was more adequate [35]. Moreover, a minor portion of H_2S was also converted to COS and CS_2 simultaneously in the presence of CH_4 and CO_2. The interaction with hydrocarbons is deemed as the third factor for H_2S consumption [15]. In this respect, Rhodes *et al.* [49] reported that the generation of COS and CS_2 could be achieved by the related reactions (Eqs. (28)–(30)) . Consequently, the H_2S concentration decayed to only about 5% at D = 3.3 and the temperature here indicated an intense combustion.

$$H_2S + OH \rightleftharpoons H_2O + SH \tag{26}$$

$$H_2S + O \rightleftharpoons H + HSO \tag{27}$$

$$CH_4 + 2H_2S \rightleftharpoons CS_2 + 4H_2 \tag{28}$$

$$CO_2 + H_2S \rightleftharpoons COS + H_2O \tag{29}$$

$$CO_2 + 2H_2S \rightleftharpoons CS_2 + 2H_2O \tag{30}$$

In the subsequent section, the remained H_2S was further oxidized and stabilized at a low level. Meanwhile, SO_2 volume fraction monotonically increased along the central axis until reaching a steady value of 26.55%, 19.26% and 15.03% in modes A, B and C, respectively. Literature reports that the generated radicals such as S, SH and HSO could be oxidized to precursor SO and finally converted to SO_2 depending on the abundance of the oxidants (Eqs. (31)–(33)) [15]. However, SO_2 was almost sparse at D = 8.3 with

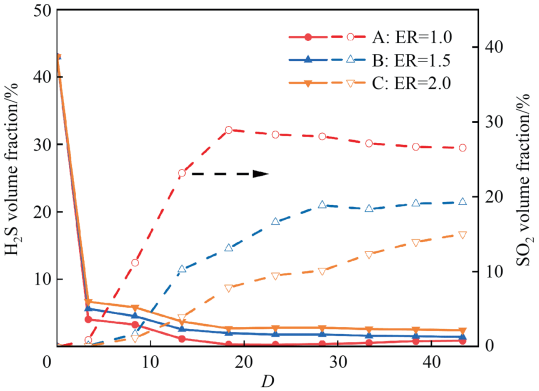

Fig. 3. Measured volume concentrations of H_2S and SO_2 along D.

only impressive concentration in mode A and its generation rate was also dependent on ER. This revealed the addition of oxidant accelerated the rate of SO_2 generation and advanced its visible position. Generally speaking, the sufficient amount of oxygen at low ER can react with H_2S to form SO_2 and H_2O in the downstream and eventually affect the final conversion and production. Additionally, the Claus reaction (Eq. (2)) occurred downstream due to the reduction or levelling off in SO_2 concentration and the presence of condensed sulfur on the reactor wall.

$$SO + OH \rightleftharpoons SO_2 + H \quad (31)$$

$$SO + SO \rightleftharpoons SO_2 + S \quad (32)$$

$$HSO + O_2 \rightleftharpoons SO_2 + OH \quad (33)$$

To declare the relationship among H_2S, CO_2 and CH_4 during combustion process, distribution of CH_4, H_2, CO and CO_2 are plotted in Figs. 4 and 5. The volume fraction of CH_4 revealed a similar trend under modes A, B and C that finally decreased to stable values of 0.07%, 1.47% and 2.57%, respectively. And the consumption of CH_4 was favored under oxidant sufficient condition. The literature reported that the decomposition was the initial conversion of CH_4 that released large amount of H and CH_3 radicals *via* Eqs. (34) and (35) [50]. It could be noted that the volume fraction of H_2 that increased promptly to the peak value at *D* of 3.3. This phenomenon verified the mentioned decomposition of H_2S and CH_4 was the essential source of hydrogen. Afterwards the partial oxidation of CH_4 occurred under the role of oxidizing medium such as O and OH radicals (Eqs. (36) and (37)) wherein limited oxygen spread from the nozzle bluff edge to the fuel stream. And the concentration of CH_4 firstly decreased by about 65% at *D* of 0–3.3. However, compared with H_2S, CH_4 tended to be converted with a less impressive rate near the nozzle and experienced a monotonic dissipation till the downstream. Though the presence of CO_2 and H_2 could somewhat inhibit the conversion of CH_4, researchers confirmed the primary factor was the oxidation competition between CH_4 and H_2S [15,51].

$$CH_4 + M \rightleftharpoons CH_3 + H + M \quad (34)$$

$$CH_4 + H \rightleftharpoons CH_3 + H_2 \quad (35)$$

$$CH_4 + OH \rightleftharpoons CH_3 + H_2O \quad (36)$$

$$CH_4 + O \rightleftharpoons CH_3 + OH \quad (37)$$

It is worthwhile to mention the study of Li *et al.* [15] regarding the oxidation competition of CH_4 and H_2S. They deemed the dominant reaction paths for CH_4 were partial oxidation and reacting

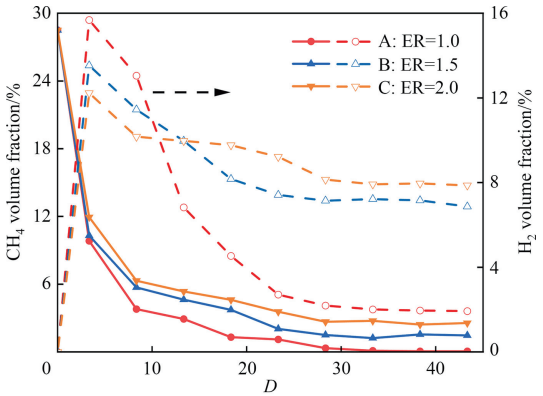

Fig. 4. Measured volume concentrations of CH_4 and CO along *D*.

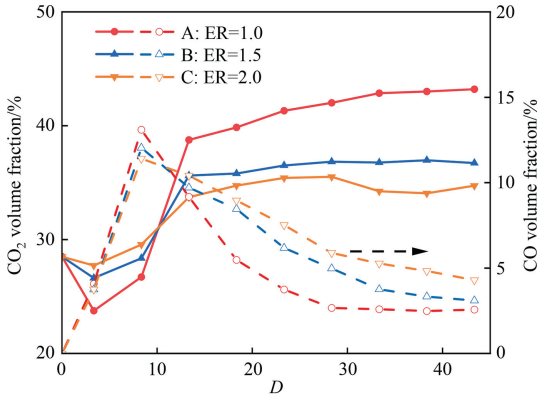

Fig. 5. Measured volume concentrations of CO_2 along *D*.

with active radicals such as S and SH through Eqs. (38) and (39). Combined with the low volume fraction of CO at *D* = 3.3, as seen in Fig. 5, this conclusion could be supported that indicated the oxidation of CH_4 was suppressed by H_2S. Meanwhile, Clark *et al.* [35,51,52] considered the initial step was the H_2S partial oxidation that produced H_2O and S_2. Subsequently CH_4 reacted with the formed sulfur species hence CS_2 and COS were produced *via* Eqs. (40) and (41).

$$CH_4 + S \rightleftharpoons CH_3 + SH \quad (38)$$

$$CH_4 + SH \rightleftharpoons CH_3 + H_2S \quad (39)$$

$$CH_4 + 2S \rightleftharpoons CS_2 + 2H_2 \quad (40)$$

$$CS_2 + H_2O \rightleftharpoons COS + H_2S \quad (41)$$

In relation to CO_2 volume fraction, it firstly decayed at *D* of 3.3 and gradually increased to a steady value. And the CO concentration featured the similar tendency to that of H_2, but reaching the peak value at a latter detected position with *D* = 8.3 and decreasing monotonically. The variation of CO_2 and CO was positively correlated with ER. It is well known that the generation of CO_2 was primarily from the further oxidation of CH_4 and CO downstream. For the CO_2 consumption at *D* of 3.3, the previous studies found that CO_2 proceeded the decomposition (Eq. (42)) to trigger the formation of CO at high temperature. In the present work, the high temperature in modes A and B would promote the reactivity of CO_2 and thus enhanced the degree of concentration attenuation. Moreover, numerous literatures indicated CO_2 could be mainly converted to CO with the help of H radical *via* Eq. (43) and attributed it to the oxidation medium impact [18,21,25,52]. This viewpoint indicated the H radical was involved in the CO_2 conversion and revealed CO_2 consumption was moderate in mode C since H_2 concentration was lower. Therefore, the number of reactions related to CO generation could be large, including the conversion of CO_2 and oxidation and steam reforming of CH_4 (Eqs. (44) and (45)). In addition, Chin *et al.* [36] considered that the presence of SO_2 could promote the CH_3 radical to CO *via* Eq. (46). However, this viewpoint could not be verified in the current work since the SO_2 concentration was not sufficient at *D* of 0–8.3.

$$CO_2 + M \rightleftharpoons CO + O + M \quad (42)$$

$$CO_2 + H \rightleftharpoons CO + OH \quad (43)$$

$$CH_4 + H_2O \rightleftharpoons CO + 3H_2 \quad (44)$$

$$2CH_4 + O_2 \rightleftharpoons 2CO + 4H_2 \quad (45)$$

$$CH_3 + SO_2 \rightleftharpoons CO + \text{products} \quad (46)$$

The distributions of CS_2 and COS volume fractions are exhibited in Figs. 6 and 7, respectively. For all the modes studied in this section, CS_2 and COS were formed rapidly at D = 3.3 wherein mixing of fuel and oxygen was not sufficient. Interestingly, the concentration of COS was higher than that of CS_2 and the rates of generation showed sensitiveness to the ER. These phenomena can be analyzed by the formation path of CS_2 and COS at relatively high temperature. Zhu *et al.* [53] considered CS_2 was primarily originated from the reactions of CH_4 and sulfur species *via* Eqs. (40) and (47). And the conversion from CO_2 to CS_2 could be complicated that the generated CO from CO_2 firstly converted into CS and further formed CS_2 [19]. Besides, Li *et al.* [15,18] concluded the formation of COS was mainly through the reactions of CO_2 and radicals like SH and S in the decomposition section (Eqs. (48) and (49)), and deemed the CO as the key precursor to react with SO and SH radicals for generating COS in the oxidation stage. And the enhancement in the COS production was found in the oxy-fuel condition with rich radicals of O and OH. Based on these studies, in the present work, it could be inferred that CS_2 was mainly formed from CH_4 instead of CO_2 near the nozzle since the C—H single bond in CH_4 was generally weaker than the C—O double bond in CO_2, and the formation of COS was possibly achieved by the interactions of CO and CO_2 with the sulfur species considering the presence of CO and consumption of CO_2 at D of 3.3. Meanwhile, the CS_2 and COS concentrations here could be explained wherein the significant presence of H_2 could inhibited the forward direction of these CS_2-formed reactions and the COS production was enhanced in the oxy-fuel condition.

$$CH + 2H_2S \rightleftharpoons CS_2 + 4H_2 \quad (47)$$

$$CO_2 + SH \rightleftharpoons COS + OH \quad (48)$$

$$CO_2 + S \rightleftharpoons COS + O \quad (49)$$

Afterwards, the volume fraction of COS decreased monotonically along the axis. It could be noted that the consumption rate of COS concentration was favored under the oxygen sufficient condition. This was attributed that the COS oxidation was the dominant channel under the role of OH, O and H radicals (reverse Eqs. (48)–(51)) [19,54]. The COS hydrolysis (reverse Eqs. (29) and (30)) was another approach that was usually considered in the first catalyst reactor of the Claus process [33]. However, the variation of CS_2 concentration decreased under ER = 1.0 and 1.5 and increased under ER = 2.0 at D > 8.3. It can be judged that CS_2 was gradually generated from CO and sulfur species in this section under oxygen deficient mode since CO was significantly present at D of 8.3. For

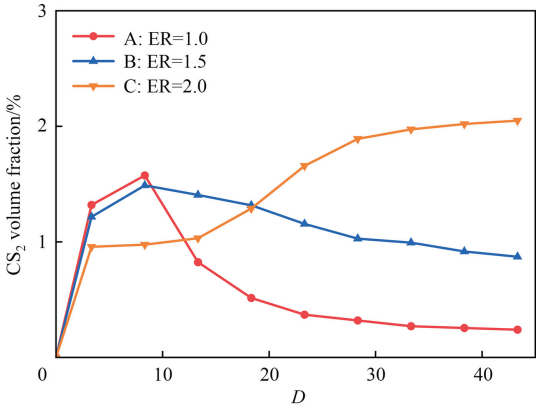

Fig. 6. Measured volume concentrations of CS_2 along D.

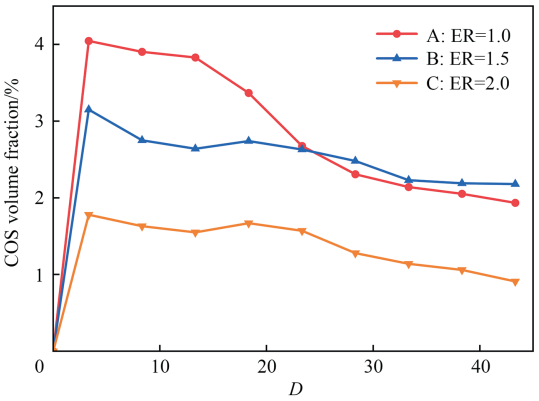

Fig. 7. Measured volume concentrations of COS along D.

the consumption of CS_2 in modes A and B, the oxidation might be accounted for the reduction in its concentration to form radicals such as CO, CS and SO *via* the reactions of Eqs. (52) and (53). Furthermore, numerous experimental and simulation studies indicated that the tight interaction of COS and CS_2 could be achieved with the aid of radicals such as SH, OH and SO (Eqs. (54) and (55)) [21,35,38,40]. The related reactions could proceed at an insignificant rate downstream of the reactor.

$$CO + SO \rightleftharpoons COS + O \quad (50)$$

$$CO + SH \rightleftharpoons COS + H \quad (51)$$

$$CS_2 + O \rightleftharpoons CS + SO \quad (52)$$

$$CS + O_2 \rightleftharpoons CO + SO \quad (53)$$

$$COS + SH \rightleftharpoons CS_2 + OH \quad (54)$$

$$COS + S_2 \rightleftharpoons CS_2 + SO \quad (55)$$

Based on the analysis of the temperature distribution and species conversion pathways under different ERs, a schematic diagram of the CH_4-AG diffusion flame was portrayed as Fig. 8. Depending on the intensity of oxidation, the whole reactor could be divided into two sections namely rapid and slow oxidation section. Meanwhile, it could also be interpreted to three zones according to various chemical process that flame inner core (0 < D < 3.3) where the initial reaction including decomposition and competitive oxidation of H_2S and CH_4 occurred, outer flame (3.3 < D < 13.3) where oxidation proceeded and subsequent complex reaction zone (13.3 < D) involving side reactions with low reaction rate.

3.2. Experimental study of CH_4-AG combustion: Effect of CH_4/AG ratio

In this section, the effect of CH_4 on AG partial oxidation was studied under ER of 1.6. Mode *D*, *E* and *F* presented here are pure oxygen with CH_4/AG of 0.3, 0.5 and 0.7. Similarly, variation of the temperature curves featured to rise to a peak value rapidly and decreased almost monotonically.

Fig. 9 reveals a positive impact of CH_4 on the axial temperature with peak values of 1000 K, 1084 K and 1123 K for modes D, E and F, respectively. This is due to the reaction heat of CH_4 is greater than that of H_2S at the same molar flow. Meanwhile, it could be noted that the temperature increment from mode D to E was significantly greater than that from modes E to F for equivariant CH_4/AG additions. Therefore, a weaker effect of added CH_4 on temperature could be predicted within high CH_4/AG region. Similarly, as discussed in the impact of ER, the added volume flow by higher

ratio of CH_4/AG showed obvious contribution on flame height and temperature gap.

The distributions of H_2S and SO_2 concentrations were summarized in Fig. 10. The volume fractions of H_2S were sharply decayed at *D* of 3.3 with increasing CH_4 proportion and the values were 9.53%, 8.48% and 6.64%, respectively. Though the flame temperature in higher CH_4/AG favored the decomposition and oxidation process of H_2S, similar effect to providing sufficient O_2, H_2S conversion was simultaneously influenced by the subsequently enhanced competitive oxidation. As seen in SO_2 profiles under CH_4/AG = 0.7, SO_2 concentration finally reached up to 23.47%, which obviously was higher than that of the other two modes. The results for the SO_2 volume fraction distributions revealed that H_2S could react preferentially with O_2 introduced by the raising of CH_4/AG. Evidently higher complete oxidation rate of H_2S could be derived under CH_4/AG enriched modes.

Figs. 11 and 12 depict the distributions of CH_4, H_2, CO_2 and CO volume fraction. It could be seen that increasing CH_4/AG had no obvious effect on the trend in concentration or conversion rate of CH_4 itself. The initial conversions of CH_4 at *D* of 3.3 for modes D–F were 62%, 68.57% and 66.53% and final conversions downstream were 96.15%, 96.68% and 95.37%, respectively. As discussed previously, oxidation of CH_4 at *D* of 3.3 was confined due to the presence of H_2S, and H_2 and COS were the typical products at flame inner core. However, the total reaction amount of CH_4 still increased with the enhancing CH_4/AG. Though the initial concentration of CO_2 (*D* = 0) decreased due to the reducing content in the fuel mixture, the final concentration of CO_2 was tightly related to CH_4/AG. Meanwhile, it is noted that discernable high concentrations of H_2 and CO, 14.89% and 12.15% are detected in CH_4/AG = 0.7 mode. The reactions of forming CO and H_2 were promoted under CH_4/AG enriched condition due to richer presence of CH_3, CH and H radicals and ultimately, higher temperature. Furthermore, the axial concentrations of H_2 and CO for all modes here were inclined to be slightly decreased and sustained downstream under anoxic atmosphere of ER = 1.6. The former Section 3.1 has emphasized that oxidation is an important process for the consumption of H_2 and CO wherein the presence of sufficient oxygen downstream is critical. Besides to it, the behavior of diffusing outward radially in the reactor and combination of CO and sulfur species may result in the slight reduction of CO concentration as seen in Eqs. (50) and (51) [18].

Figs. 13 and 14 show the distributions of CS_2 and COS concentration under investigated modes. It exhibited CS_2 and

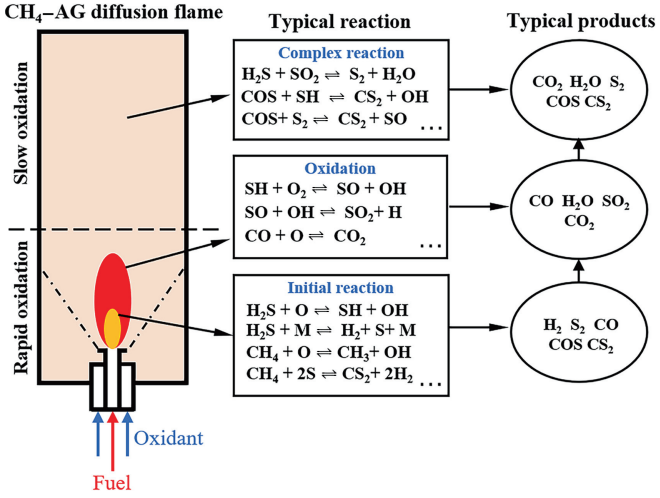

Fig. 8. Schematic diagram of CH_4–AG diffusion flame under oxy-fuel condition.

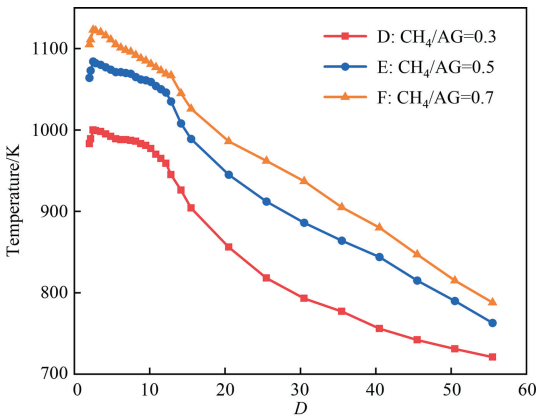

Fig. 9. Measured temperature profiles *versus* CH_4/AG.

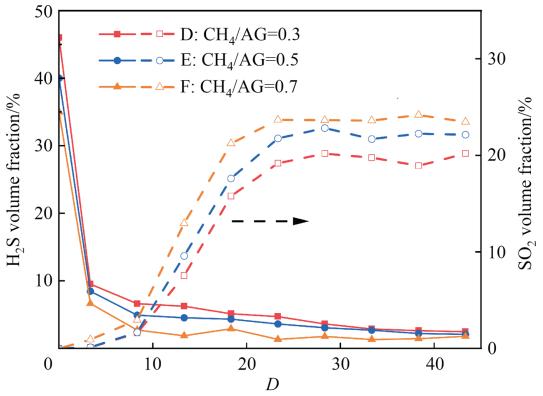

Fig. 10. Measured volume concentrations of H_2S and SO_2 along *D*.

COS experienced rapid generation at flame inner area and moderate consumption in the latter section of the reactor. It is interesting that CS_2 and COS formation were higher in mode E during the flame zone and the final concentrations downstream were dependent on the CH_4/AG ratio. This showed that suitable concentration of reactants was the key to generate CS_2 and COS. And the high richness of carbon and sulfur species was more likely to maintain the CS_2 and COS concentration downstream. Meanwhile, the striking distinction was the noticeably lower formation of COS in the CH_4/AG = 0.3 case. This observation coincides with the remarkable lowest temperature, but also lowest concentration of CS_2 in mode D. As has been discussed that low temperature hinders CH_4 and

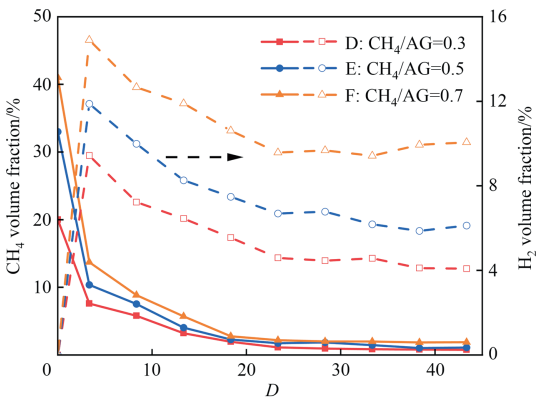

Fig. 11. Measured volume concentrations of CH_4 and H_2 along *D*.

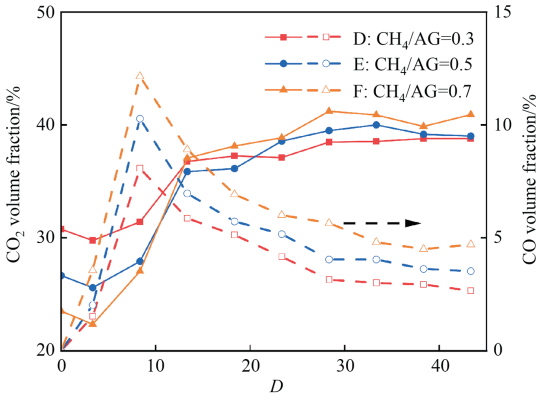

Fig. 12. Measured volume concentrations of CO_2 along D.

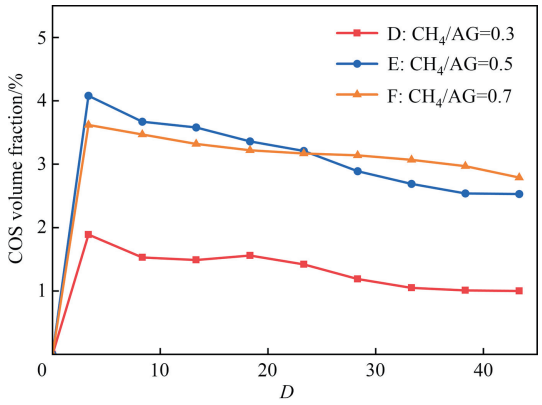

Fig. 14. Measured volume concentrations of COS along *D*.

H_2S decomposition, CH and SH radicals generation and CO production, and these factors, aside from the lower reaction rate, are negative for the CS_2 and COS formation through mentioned reaction paths.

4. Conclusions

In the current study, the combustion of methane and acid gas was conducted in a diffusion flame *via* a coaxial burner. The distribution of the flame temperature and main species concentration on the central axis were analyzed under different equivalence ratios and CH_4-addition ratios. The CH_4–AG diffusion flame under oxy-fuel combustion was described and the conversion and generation of species were discussed.

Generally, the CH_4–AG diffusion flame could be divided into three sections according to the distinct chemical processes namely the initial reaction, oxidation and complex reaction sections. During the first section, the decomposition and partial oxidation of H_2S and CH_4 occurred wherein large amount of H_2 were produced. Oxidation competition could also be found here that the CH_4 conversion was inferior to that of H_2S. CH_4 could interact with sulfur species that contributed to formations of COS and CS_2. Meanwhile CO_2 was initially consumed here mainly *via* $CO_2 + H \rightarrow CO + OH$ and subsequently generated from the complete oxidation of CH_4 and CO wherein mixing of the fuel and oxidant became adequate. The production of SO_2 was improved and advanced under sufficient oxygen condition while its obvious appearance would be postponed to the oxidation section and the final volume fraction would be promoted by reducing ER and increasing CH_4/AG. The generations of H_2 and CO were favored by this trend. However, the formed H_2 and CO could be consumed mainly through oxidation reaction downstream for mode A while they were inclined to be sustained in mode B–F.

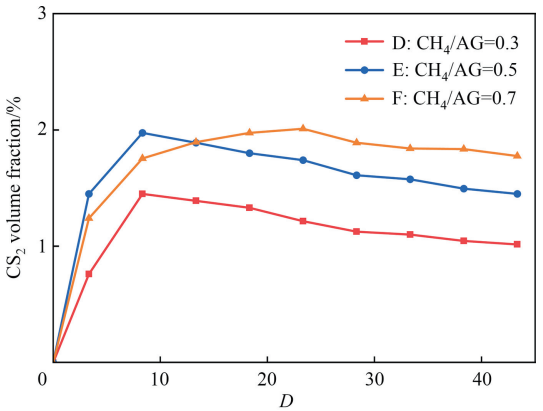

Fig. 13. Measured volume concentrations of CS_2 along *D*.

COS and CS_2 experienced rapid generation at flame inner area. COS was mainly formed by interactions of CO and CO_2 with sulfur species. And production of CS_2 directly relied on the reaction of CH_4 with sulfur species. With low ER and high CH_4/AG application, generation rates of COS and CS_2 were increased under higher temperature and enhancing carbon–sulfur–oxygen environment. The concentration of COS was higher than that of CS_2 since the large presence of H_2 prevented the main paths of CS_2 generation. COS and CS_2 could be consumed by oxidation process and the decay rates were closely related to ER.

Considering the heat resistance of the materials in the practical Claus furnace, CH_4 co-combustion and oxy-fuel combustion are rarely applied simultaneously since high temperatures can be achieved. However, the unequal state of CH_4 in AG oxidation remains unchanged and the generation of COS and CS_2 contaminants is significant in the flame inner core. As enhanced conditions, it may provide references for the suitable applications of CH_4 co-combustion, oxy-fuel combustion and fitting ER in the Claus furnace, which can meet requirements including control of furnace temperature, improvement of species conversion and reduction of COS and CS_2. Meanwhile, the selection of proper conditions, such as ER = 1.6, CH_4/AG = 0.7 in this study and suitable reactor length, may achieve the production of valuable syngas (CO and H_2) directly from CH_4–AG combustion after exhaust gas separation.

Data Availability

Data will be made available on request.

Declaration of Competing Interest

The authors declare that they have no known competing financial interests or personal relationships that could have appeared to influence the work reported in this paper.

Acknowledgements

The project was supported by the National Natural Science Foundation of China (21978092).

Nomenclature

C_p	specific heat capacity, $J \cdot K^{-1} \cdot mol^{-1}$
D	dimensionless axial distance
E_{CH_4}	uncertainty of CH_4, %

$E_{CH_4/AG}$ uncertainty of the CH_4/AG ratio, %
E_{ER} uncertainty of the equivalence ratio, %
E_{H_2S} uncertainty of H_2S, %
E_{O_2} uncertainty of O_2, %
h_f convective heat transfer coefficient, $W \cdot m^{-2} \cdot K^{-1}$
m_{fuel} mass flow rate of H_2S, $kg \cdot min^{-1}$
m_{O_2} mass flow rate of O_2, $kg \cdot min^{-1}$
Nu Nussle number
P_i production of species i, %
Pr Prandtl number
Re Reynolds number
S_i product selectivity of species i, %
T_b electric coupling bead temperature, K
T_g gas temperature, K
T_w reactor wall temperature, K
V_{CH_4} volume flow rate of CH_4, $L \cdot min^{-1}$
V_{H_2S} volume flow rate of H_2S, $L \cdot min^{-1}$
V_{O_2} volume flow rate of O_2, $L \cdot min^{-1}$
δV flow rate controlling resolution, $L \cdot min^{-1}$
ε emission rate
μ kinetic viscosity, Pa·s
σ blackbody radiation constant, $W \cdot m^{-2} \cdot K^{-4}$
φ relative error

References

[1] J.S. Eow, Recovery of sulfur from sour acid gas: A review of the technology, *Environ. Prog.* 21 (3) (2002) 143–162.
[2] O. Abed Habeeb, R. Kanthasamy, G.A.M. Ali, S. Sethupathi, R. Bin Mohd Yunus, Hydrogen sulfide emission sources, regulations, and removal techniques: A review, *Rev. Chem. Eng.* 34 (6) (2018) 837–854.
[3] J.S. Lar, X.J. Li, Removal of H_2S during anaerobic bioconversion of dairy manure, *Chin. J. Chem. Eng.* 17 (2) (2009) 273–277.
[4] J.F. Zhang, Z.Q. Tong, H_2S removal with cupric chloride for producing sulfur, *Chin. J. Chem. Eng.* 14 (6) (2006) 810–813.
[5] A.K. Gupta, S. Ibrahim, A. Al Shoaibi, Advances in sulfur chemistry for treatment of acid gases, *Prog. Energy Combust. Sci.* 54 (2016) 65–92.
[6] X.H. Lü, H. Li, X.H. Du, X.E. Wang, M.Y. Lan, J.L. Wu, J. Zhu, J.L. Sun, F. Jiang, Simultaneous catalytic reduction of SO_2 and NO from flue gas using H_2S as a reductant at low temperatures, *React. Chem. Eng.* 5 (3) (2020) 561–569.
[7] S. Sinha, A. Raj, A.S. AlShoaibi, S.M. Alhassan, S.H. Chung, Toluene destruction in the Claus process by sulfur dioxide: A reaction kinetics study, *Ind. Eng. Chem. Res.* 53 (42) (2014) 16293–16308.
[8] R. Schmidt, J.B. Cross, E.G. Latimer, Tail-gas cleanup by simultaneous SO_2 and H_2S removal, *Energy Fuels* 23 (7) (2009) 3612–3616.
[9] I.A. Gargurevich, Hydrogen sulfide combustion: Relevant issues under Claus furnace conditions, *Ind. Eng. Chem. Res.* 44 (20) (2005) 7706–7729.
[10] A. Mehmood, H. Alhasani, N. Alamoodi, Y.F. AlWahedi, S. Ibrahim, A. Raj, An evaluation of kinetic models for the simulation of Claus reaction furnaces in sulfur recovery units under different feed conditions, *J. Nat. Gas Sci. Eng.* 74 (2020) 103106.
[11] F. Manenti, D. Papasidero, A. Frassoldati, G. Bozzano, S. Pierucci, E. Ranzi, Multi-scale modeling of Claus thermal furnace and waste heat boiler using detailed kinetics, *Comput. Chem. Eng.* 59 (2013) 219–225.
[12] M. Frenklach, J.H. Lee, J.N. White, W.C. Gardiner, Oxidation of hydrogen sulfide, *Combust. Flame* 41 (1981) 1–16.
[13] H. Selim, S. Ibrahim, A. Al Shoaibi, A.K. Gupta, Investigation of sulfur chemistry with acid gas addition in hydrogen/air flames, *Appl. Energy* 113 (2014) 1134–1140.
[14] H. Kazempour, F. Pourfayaz, M. Mehrpooya, Modeling and multi-optimization of thermal section of Claus process based on kinetic model, *J. Nat. Gas Sci. Eng.* 38 (2017) 235–244.
[15] Y. Li, Q.H. Guo, Z.H. Dai, Y.C. Dong, G.S. Yu, F.C. Wang, Study of oxidation for gas mixture of H_2S and CH_4 in a non-premixed flame under oxygen deficient condition, *Appl. Therm. Eng.* 117 (2017) 659–667.
[16] A. Raj, S. Ibrahim, A. Jagannath, Combustion kinetics of H_2S and other sulfurous species with relevance to industrial processes, *Prog. Energy Combust. Sci.* 80 (2020) 100848.
[17] Y.L. Xie, J.H. Wang, M. Zhang, J. Gong, W. Jin, Z.H. Huang, Experimental and numerical study on laminar flame characteristics of methane oxy-fuel mixtures highly diluted with CO_2, *Energy Fuels* 27 (10) (2013) 6231–6237.
[18] Y. Li, Q.H. Guo, X.L. Yu, Z.H. Dai, Y.F. Wang, G.S. Yu, F.C. Wang, Effect of O_2 enrichment on acid gas oxidation and formation of COS and CS_2 in a rich diffusion flame, *Appl. Energy* 206 (2017) 947–958.
[19] M. Abián, M. Cebrián, Á. Millera, R. Bilbao, M.U. Alzueta, CS_2 and COS conversion under different combustion conditions, *Combust. Flame* 162 (5) (2015) 2119–2127.
[20] Y. Li, X.L. Yu, H.J. Li, Q.H. Guo, Z.H. Dai, G.S. Yu, F.C. Wang, Detailed kinetic modeling of homogeneous H_2S–CH_4 oxidation under ultra-rich condition for H_2 production, *Appl. Energy* 208 (2017) 905–919.
[21] Y. Li, X.L. Yu, H.J. Li, Q.H. Guo, Z.H. Dai, G.S. Yu, F.C. Wang, Detailed kinetic modelling of H_2S oxidation with presence of CO_2 under rich condition, *Appl. Energy* 190 (2017) 824–834.
[22] S.M. Wang, D. Wu, H.L. Huang, Q.Y. Yang, M.M. Tong, D.H. Liu, C.L. Zhong, Computational exploration of H_2S/CH_4 mixture separation using acid-functionalized UiO-66(Zr) membrane and composites, *Chin. J. Chem. Eng.* 23 (8) (2015) 1291–1299.
[23] Y. Li, Z.H. Dai, Y.C. Dong, J.L. Xu, Q.H. Guo, F.C. Wang, Equilibrium prediction of acid gas partial oxidation with presence of CH_4 and CO_2 for hydrogen production, *Appl. Therm. Eng.* 107 (2016) 125–134.
[24] D. Bongartz, A.F. Ghoniem, Chemical kinetics mechanism for oxy-fuel combustion of mixtures of hydrogen sulfide and methane, *Combust. Flame* 162 (3) (2015) 544–553.
[25] H. Selim, A.K. Gupta, A. Al Shoaibi, Effect of CO_2 and N_2 concentration in acid gas stream on H_2S combustion, *Appl. Energy* 98 (2012) 53–58.
[26] S. Ibrahim, A. Raj, Kinetic simulation of acid gas (H_2S and CO_2) destruction for simultaneous syngas and sulfur recovery, *Ind. Eng. Chem. Res.* 55 (24) (2016) 6743–6752.
[27] C.E. Lee, S.R. Lee, J.W. Han, J. Park, Numerical study on effect of CO_2 addition in flame structure and NO_x formation of CH_4–air counterflow diffusion flames, *Int. J. Energy Res.* 25 (4) (2001) 343–354.
[28] J. Berner-Cambot, C. Vovelle, R. Delbourgo, Flame structures of H_2S–air diffusion flames, *Symp. Int. Combust.* 18 (1) (1981) 777–783.
[29] K. Karan, L.A. Behie, CS_2 formation in the Claus reaction furnace: A kinetic study of methane–sulfur and methane–hydrogen sulfide reactions, *Ind. Eng. Chem. Res.* 43 (13) (2004) 3304–3313.
[30] J.M. Colom-Díaz, M. Leciñena, A. Peláez, M. Abián, R. Millera, M.U.A. Bilbao, Study of the conversion of CH_4/H_2S mixtures at different pressures, *Fuel* 262 (2020) 116484.
[31] S. Ibrahim, A. Al Shoaibi, A.K. Gupta, Role of toluene to acid gas (H_2S and CO_2) combustion in H_2/O_2–N_2 flame under Claus condition, *Appl. Energy* 149 (2015) 62–68.
[32] S. Ibrahim, A. Al Shoaibi, A.K. Gupta, Effect of benzene on product evolution in a H_2S/O_2 flame under Claus condition, *Appl. Energy* 145 (2015) 21–26.
[33] S. Ibrahim, A. Al Shoaibi, A.K. Gupta, Xylene addition effects to H_2S combustion under Claus condition, *Fuel* 150 (2015) 1–7.
[34] V. Palma, V. Vaiano, D. Barba, M. Colozzi, E. Palo, L. Barbato, S. Cortese, H_2 production by thermal decomposition of H_2S in the presence of oxygen, *Int. J. Hydrog. Energy* 40 (1) (2015) 106–113.
[35] H. Selim, A. Al Shoaibi, A.K. Gupta, Effect of H_2S in methane/air flames on sulfur chemistry and products speciation, *Appl. Energy* 88 (8) (2011) 2593–2600.
[36] H.S.F. Chin, K. Karan, A.K. Mehrotra, L.A. Behie, The fate of methane in a Claus plant reaction furnace, *Can. J. Chem. Eng.* 79 (4) (2001) 482–490.
[37] P.D. Clark, N.I. Dowling, M. Huang, W.Y. Svrcek, W.D. Monnery, Mechanisms of CO and COS formation in the Claus furnace, *Ind. Eng. Chem. Res.* 40 (2) (2001) 497–508.
[38] K. Karan, A.K. Mehrotra, L.A. Behie, A high-temperature experimental and modeling study of homogeneous gas-phase COS reactions applied to Claus plants, *Chem. Eng. Sci.* 54 (15–16) (1999) 2999–3006.
[39] P. Glarborg, B. Halaburt, P. Marshall, A. Guillory, J. Troe, M. Thellefsen, K. Christensen, Oxidation of reduced sulfur species: Carbon disulfide, *Chem. A Eur. J.* 118 (34) (2014) 6798–6809.
[40] P.D. Clark, N.I. Dowling, M. Huang, Conversion of CS_2 and COS over alumina and titania under Claus process conditions: Reaction with H_2O and SO_2, *Appl Catal B* 31 (2) (2001) 107–112.
[41] L.G. Blevins, W.M. Pitts, Modeling of bare and aspirated thermocouples in compartment fires, *Fire Saf. J.* 33 (4) (1999) 239–259.
[42] D. Green, M. Southard, Perry's Chemical Engineers' Handbook, ninth ed., McGraw-Hill, New York, USA, 2019.
[43] S. Whitaker, Forced convection heat transfer correlations for flow in pipes, past flat plates, single cylinders, single spheres, and for flow in packed beds and tube bundles, *AIChE J* 18 (2) (1972) 361–371.
[44] V. Kaloidas, N. Papayannakos, Kinetics of thermal, non-catalytic decomposition of hydrogen sulphide, *Chem. Eng. Sci.* 44 (11) (1989) 2493–2500.
[45] H. Selim, S. Ibrahim, A. Al Shoaibi, A.K. Gupta, Effect of oxygen enrichment on acid gas combustion in hydrogen/air flames under Claus conditions, *Appl. Energy* 109 (2013) 119–124.
[46] K.A. Hawboldt, W.D. Monnery, W.Y. Svrcek, New experimental data and kinetic rate expression for H_2S pyrolysis and re-association, *Chem. Eng. Sci.* 55 (5) (2000) 957–966.
[47] A. Stagni, S. Arunthanayothin, L. Pratali Maffei, O. Herbinet, F. Battin-Leclerc, T. Faravelli, An experimental, theoretical and kinetic-modeling study of hydrogen sulfide pyrolysis and oxidation, *Chem. Eng. J.* 446 (2022) 136723.
[48] P.D. Clark, M. Huang, S. Liu, X. Long, Partial oxidation of hydrogen sulphide in the manufacture of hydrogen, sulphur, ethylene and propylene, *Sulphuric Acid Ind.* 4 (2004) 1–8.
[49] C. Rhodes, S.A. Riddel, J. West, B.P. Williams, G.J. Hutchings, The low-temperature hydrolysis of carbonyl sulfide and carbon disulfide: A review, *Catal. Today* 59 (3–4) (2000) 443–464.
[50] A.M. El-Melih, L. Iovine, A. Al Shoaibi, A.K. Gupta, Production of hydrogen from hydrogen sulfide in presence of methane, *Int. J. Hydrog. Energy* 42 (8) (2017) 4764–4773.

[51] H. Selim, A. Al Shoaibi, A.K. Gupta, Fate of sulfur with H_2S injection in methane/air flames, *Appl. Energy* 92 (2012) 57–64.
[52] D.V. Demidov, I.V. Mishin, M.N. Mikhailov, Gibbs free energy minimization as a way to optimize the combined steam and carbon dioxide reforming of methane, *Int. J. Hydrog. Energy* 36 (10) (2011) 5941–5950.
[53] T.L. Zhu, A. Dreher, M. Flytzani-Stephanopoulos, Direct reduction of SO_2 to elemental sulfur by methane over ceria-based catalysts, *Appl Catal B* 21 (2) (1999) 103–120.
[54] Y. Murakami, M. Kosugi, K.J. Susa, T. Kobayashi, N. Fujii, Kinetics and mechanism for the oxidation of CS_2 and COS at high temperature, *Bull. Chem. Soc. Jpn* 74 (7) (2001) 1233–1240.